RSC Advances

PAPER

View Article Online
View Journal | View Issue

Cite this: *RSC Adv.*, 2024, **14**, 32786

Observation of excellent photocatalytic and antibacterial activity of Ag doped ZnO nanoparticles

Vaishali Amrute,[a] Monika,[a] K. K. Supin,[bc] M. Vasundhara[*bc] and Anupama Chanda[*a]

Nanotechnology is the platform with the greatest promise for scientific advancements. One of the advancement is improvement in photocatalytic and antibacterial performance. This work was undertaken to synthesize un-doped and silver (Ag) doped zinc oxide (ZnO) nanoparticles (NPs) using an inexpensive wet chemical method and to investigate the structural and optical properties, photocatalytic and antibacterial activity. The structural analysis from X-ray diffraction (XRD) pattern of un-doped and Ag-doped ZnO NPs displayed hexagonal wurtzite crystal structure and shifting in the peak position confirms the incorporation of Ag in ZnO lattice. Morphological study done by scanning electron microscope reveals spherical shaped NPs and an increase in grain size with Ag doping, the HRTEM images showed the nanocrystalline nature of particle. The Raman spectra showed variation in vibrational characteristics of the nanoparticles with Ag doping. The functional groups were analyzed using Fourier transform-infrared spectroscopy (FTIR). The optical properties were investigated by UV-visible and photoluminescence (PL) spectroscopic techniques. The Ag-doped ZnO NPs have a notably lower band gap than that of un-doped ZnO NPs, *i.e.* from 3.04 eV to 2.81 eV as studied by UV-visible spectra. The PL study showed decrease in intensity at near band edge emission with increase in Ag doping concentration indicating reduction in the free charge carrier recombination. These variations in the properties play major role in the enhancement of photocatalytic and antibacterial activity with increase in Ag doping concentration as compared to un-doped zinc oxide nanoparticles. The photo degradation efficiency of 99.12 ± 1% against Methylene Blue dye was achieved in the shortest period of 45 minutes ever reported when irradiated under the solar light and efficiency of 97.33 ± 1% was achieved in 15 min under Xenon Short Arc lamp. The antibacterial study was conducted using the Agar well diffusion method where the diameter of the zone of inhibition (ZOI) was increased from 14 mm to 20 mm and 13 mm to 18 mm against the bacteria *Escherchia coli* and *Bacillus subtilis* respectively, rendering this material suitable for photocatalytic degradation and antibacterial applications.

Received 17th July 2024
Accepted 26th September 2024

DOI: 10.1039/d4ra05197a

rsc.li/rsc-advances

Introduction

Nanotechnology[1] has emerged as a powerful tool for advancing materials science and addressing critical challenges across various fields. Scaling down a material from macro to nano size has significant effects on its properties, such as optical, magnetic, electrical, antibacterial, and mechanical properties, among others. Nanoparticles (NPs) are defined as particles with a diameter varying from 1 to 100 nm[2]. The development of metal oxide nanostructures, including TiO_2, ZnO, SnO_2, MnO_2, Co_3O_4, Fe_2O_3, NiO, has a significant impact in material science and many other fields due to their extraordinary physiochemical properties, such as density, melting/boiling points, electrical conductivity, magnetism, basicity, and reactivity *etc.*[3–8]Among all metal oxides, ZnO stands out as a significant nanomaterial because of its excellent optoelectronics, piezoelectric, gas sensing, photocatalytic, and antibacterial properties. These properties are attributed to unique characteristics like a broad energy gap of 3.37 eV, high intrinsic electron mobility of 300 $cm^2 V^{-1} s^{-1}$, large excitonic binding energy of 60 meV, a melting point as high as 2248 K, and a cohesive energy of 1.89 eV.[9–12] Photocatalysis emerges as one of the most efficient and sustainable approach for environmental remediation, enabling the decomposition of pollutants by harnessing solar energy.[13,14] Among these pollutants, the cationic compound Methylene blue (MB), a common dye used in various industries has been found to be toxic and hazardous to the environment.[15–17] Additionally, antibacterial strategies aim to

[a]*Department of Physics, Dr. Harisingh Gour Vishwavidyalaya (A Central University), Sagar, M.P. 470003, India. E-mail: achanda@dhsgsu.edu.in*

[b]*Polymers and Functional Materials Department, CSIR-Indian Institute of Chemical Technology, Hyderabad 500007, India. E-mail: mvas@iict.res.in*

[c]*Academy of Scientific and Innovative Research (AcSIR), Ghaziabad 201002, India*

tackle the challenges posed by bacterial infections, which remain a constant threat to global health. Although ZnO exhibits promising qualities as a photocatalytic, biocompatible, and antibacterial agent, the rapid recombination of photogenerated electron–hole pairs presents a constraining factor that retards the activity of ZnO NPs. In response to this challenge, significant efforts have been devoted to improvement. Doping ZnO NPs with metals has demonstrated effectiveness in producing highly active reactive agents. ZnO doped with metals like Ni, Mn, Fe, Co, Cr and Ag and synthesized *via* hydrothermal method show good photocatalytic activity due to narrowing of the band gap.[18,19] Doping with other novel metals with suitable work functions, such as Pt, Pd, Au also increases photodegradation and antimicrobial efficiency.[20–23] Currently, the production of Ag-doped ZnO NPs has become an exciting area of research for both photocatalytic and antibacterial activities. Among all the metals/novel metals Ag shows better enhancement in both the activities. Since the band gap of ZnO is relatively large, the integration of Ag ions (Ag^+) in ZnO host lattice enhances absorption capacity, improves charge separation capabilities, and offers significant potential for enhancement. Ag NPs have been utilized for degradation of pollutants found in industrial waste and control of bacterial growth on various materials such as medical devices, dental composite materials, and textiles. Silver (Ag) can enhance the photocatalytic activity of ZnO nanoparticles by improving surface properties such as O vacancies, crystal deficiencies and increased specific surface area.[24] The reported photodegradation efficiency due to reactive oxygen species (ROS) production and band gap of Ag-doped ZnO NPs was 98% in 120 minutes.[1] Various studies reported the degradation efficiency of 89% at 140 min[25] of Ag-doped ZnO NPs against ponceau, removal of CB dye about 65% after 120 min,[26] 100% degradation efficiency against MB dye after 300 minutes,[27] 2% increase in degradation efficiency on Ag doped ZnO compared to ZnO against the MV dye.[28] The antibacterial activity against the bacterial strain of *Escherichia coli*, *Bacillus subtilis*, *Pseudomonas aeruginosa*, *Staphylococcus aureus*, *Enterococcus faecalis* were also reported.[2,29,30] Surface characteristics, including oxygen vacancies and crystal defects contribute to the enhanced photocatalytic and antibacterial activity of the particles.[31,32] Consequently, Ag-doped ZnO NPs have been utilized as both photocatalytic and antibacterial agents owing to the alteration in crystallite size/particle size resulting from the incorporation of Ag into the ZnO lattice. Ag NPs exhibit a large surface-to-volume ratio, which enhances their effectiveness in supporting these activities.

Several methods have been employed for the development of ZnO NPs, including the sol–gel method,[33,34] hydrothermal and solvothermal methods,[35,36] electrochemical method[37] microwave method[38,39] and others. Yet, these methods often entail significant time and complexity. The current study primarily emphasizes a simple and cost-effective synthesis technique for un-doped and Ag-doped ZnO NPs using the wet chemical method. While there is an abundance of literature on nanoparticle synthesis *via* the wet chemical route, only a limited number of studies offer comprehensive analysis of the photocatalytic and antibacterial activity of Ag-doped ZnO NPs. This study reports a photodegradation efficiency of 99.12 ± 1% in Ag-doped ZnO NPs within 45 minutes, and 97.33 ± 1% in 15 min under solar light and Xenon Short Arc lamp respectively marking the shortest span ever reported. The objective of this approach is to explore the structural and optical properties, as well as the photocatalytic activity for degrading MB and the antibacterial effectiveness against bacterial strains, including Gram-negative *Escherichia coli* and Gram-positive *Bacillus Subtilis*, of Ag-doped ZnO NPs.

Experimental procedure

Materials

Un-doped and Ag-doped ZnO (Ag/ZnO) NPs were synthesized using the following chemicals: zinc acetate ($Zn(CH_3COO)_2 \cdot 2H_2O$, 98.0%, M.W. – 219.50, Lobagens), sodium hydroxide pellets (NaOH, 98.0%, M.W. – 40, Himedia), silver nitrate ($AgNO_3$, M.W. – 169.87, Fisher), and deionized (DI) water, which was also used in the experiment.

Synthesis method

Un-doped and Ag-doped ZnO (with Ag at. wt%: 1, 3, 5 and 7%) NPs were synthesized using the wet chemical method. For ZnO synthesis, a 1 M solution was prepared through dissolution of zinc acetate ($(CH_3COO) \cdot 2Zn \cdot 2H_2O$) in 50 ml of deionized (DI) water, stirred for 30 minutes. Another solution of the reducing agent, 1 M NaOH, was prepared. After 30 minutes, this solution was gradually introduced to the zinc acetate solution under the same stirring conditions until a white precipitate formed, maintaining a pH of 5–6. The solution was subsequently stirred for two hours at ambient temperature. Once the precipitate had fully formed, the solid and liquid phases were separated employing a centrifuge for 10 minutes at 6000 rpm. The precipitate was washed 3–4 times with deionized water and ethanol to remove impurities, subsequently dried in an oven for 20 hours at 80 °C. The dried precipitate was then ground, and finally, the resulting powder was annealed in a muffle furnace at 400 °C for 2 hours, producing un-doped ZnO NPs. For the synthesis of Ag-doped ZnO NPs, the required amount of silver nitrate ($AgNO_3$), corresponding to the doping at. wt% (1%, 3%, 5%, 7%), was added to the zinc acetate solution in the above reaction. The entire procedure remained the same. Finally, Ag/ZnO NPs were formed with various concentrations of Ag at. wt%. Henceforth Ag-doped ZnO NPs ($Zn_{1-x}Ag_xO$:$X = 0.01$, 0.03, 0.05, 0.07) are denoted as AZO-1, AZO-3, AZO-5, AZO-7 respectively.

Characterization techniques

X-ray diffraction (XRD) patterns of the samples, utilized for phase identification and crystallinity determination, were obtained using a Bruker D8 Advance X-ray powder diffraction technique. CuKα radiation with a wavelength (λ) of 1.5404 Å was employed. A scanning electron microscope (SEM) specifically the NOVA NANOSEM 450 was utilized for morphological analysis. Elemental composition was studied using energy dispersive X-ray (EDX) analysis with the help of a NOVA NANOSEM 450

microscope working at a 200 kV accelerating voltage, Microstructure study was carried out using a transmission electron microscope (G2F30S – Twin model of HRTEM). The RAMAN analysis was done by LABRAM-HR 800 (Horibra) RAMAN spectrometer having a diode laser source of wavelength 473 nm. Bruker Alfa II instrument was employed for Fourier transforms infrared (FTIR) spectra analysis. Optical analysis was conducted using a Shimadzu UV 2401 PC spectrophotometer. Additionally, photoluminescence (PL) spectra were captured using a Spectro fluorophotometer, namely the Horiba Scientific Instrument Fluoromax-4 spectrofluorometer. A spectral slit width of 3.0 nm was used, and a 450 W xenon arc lamp served as the exciting source.

Photocatalytic studies

The photocatalytic experimental set-up was developed by exposing reaction mixture (Photocatalyst-MB dye solution) in sunlight under constant stirring of 500 rpm in a magnetic stirrer. Solar light intensity was gauged using a Lux meter. 5 mg of catalyst was introduced into the 50 mL of 10^{-5}M MB dye solution. The solution was then stirred continuously under sunlight. At a regular interval of 15 minutes, 5 mL of reaction mixture was extracted using a micropipette by switching off the stirring process. Till 90 minutes, 6 such aliquots were taken and each mixture was centrifuged at 10 000 rpm for 10 minutes. The same experiment was also performed using Xenon Short Arc lamp (150 watt, Air cooling) under constant magnetic stirring of 500 rpm. Here, samples were collected at a regular time interval of 5 minutes. The solution was then centrifuged at 10 000 rpm. Then, each mixture was then analysed using the UV-visible spectroscopy over the wavelength range of 200–800 nm, to verify the absorbance values. The change in absorbance values is the guidance towards the MB degradation studies.

Antibacterial studies

For assessing the antibacterial potential of un-doped and Ag-doped nanoparticles, Agar well-diffusion method was employed. The antibacterial potency of nanoparticles was assessed on nutrient agar plates against *E. coli* and *B. subtilis*. The bacterial suspension was evenly distributed on the plates and 100 μL un-doped and Ag-doped ZnO NPs of suspension was poured on 6 mm wells made on agar surface from sterile cork borer. DI water was taken as a control. Plates were then incubated at 37 °C for 24 h and the inhibition zone was measured.

Results and discussion

X-ray diffraction examination

The structural analysis of un-doped and Ag-doped ZnO NPs was done using X-ray diffraction (XRD) technique. The XRD patterns of both un-doped and Ag-doped ZnO NPs, as shown in Fig. 1a, reveal that ZnO and AZO-1, AZO-3, AZO-5, AZO-7 exhibit hexagonal wurtzite structure, confirming in accordance with JCPDS No.- 800 075. The diffraction peaks of ZnO NPs, observed at 2θ angles of 31.55, 34.21, 36.05, 47.38, 56.39, 62.69, 66.22, 67.77, and 68.94°, correspond to the diffraction planes (100), (002), (101), (102), (110), (103), (200), (112), and (201), respectively. The sharp and intense diffraction peaks indicate the crystalline nature of NPs. In the Ag-doped ZnO pattern, a right shift in the diffraction peak position was noted (Fig. 1b), which confirms the integration of Ag^{+} ions into the ZnO host lattice. This shift is attributed to the larger ionic radius of Ag^{+} (0.126 nm) compared to Zn^{2+} (0.074 nm). Upon Ag doping in the ZnO lattice, additional diffraction peaks at 37.97°, 44.17°, and 64.32° due to Ag were detected for higher Ag concentrations (3, 5 and 7 at%).

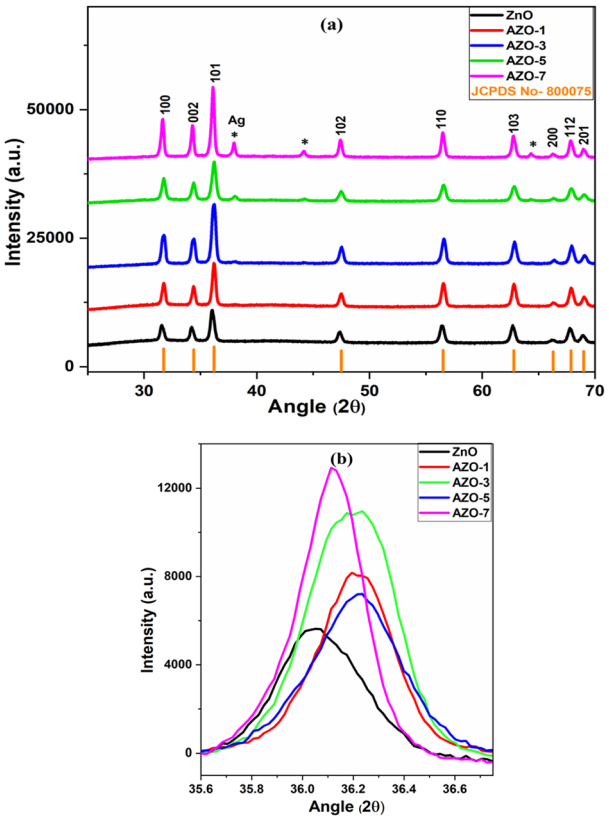

Fig. 1 (a) XRD pattern of un-doped ZnO and Ag-doped ZnO (AZO-1 to AZO-7) NPs (b) enlarged view of XRD peak corresponding to diffraction plane (101).

To investigate the impact of Ag dopant on the crystallite size (D), the Debye–Scherrer equation (eqn (1)) was utilized for estimating the crystallite size, as outlined in Table 1.

$$D = k\lambda/\beta\cos\theta \quad (1)$$

where $k = 0.9$, X-ray wavelength $\lambda = 1.54$ Å, β = FWHM, θ = Bragg angle. With increase in Ag content the crystallite size increases for AZO-1 but after that it decreases for AZO-3 and AZO-5 and again it increases for AZO-7 sample. The increase in crystallite size may have attributed to ionic size difference between the Ag^{+} (0.126 nm) and Zn^{2+} (0.074 nm) ions.[28] In AZO-1, there is substitution of Ag ions on Zn^{2+} ions and due to ionic size difference the crystallite size may have increased. The crystallite size decreases due to the lattice stress induced by the presence of Ag within the ZnO structure.[40] Due to incorporation

Table 1 Parameters derived from XRD analysis

	For miller diffraction plane (101)				
Sample	FWHM	*d*-spacing (Å)	Crystallite size *D* (nm)	Dislocation density ($\delta \times 10^{-3}$)	Microstrain ($\varepsilon \times 10^{-3}$)
ZnO	0.406	2.487	20.55	2.367	5.445
AZO-1	0.353	2.478	23.68	1.784	4.709
AZO-3	0.405	2.479	20.61	2.354	5.412
AZO-5	0.427	2.478	19.56	2.613	5.7
AZO-7	0.318	2.484	26.31	1.444	4.249

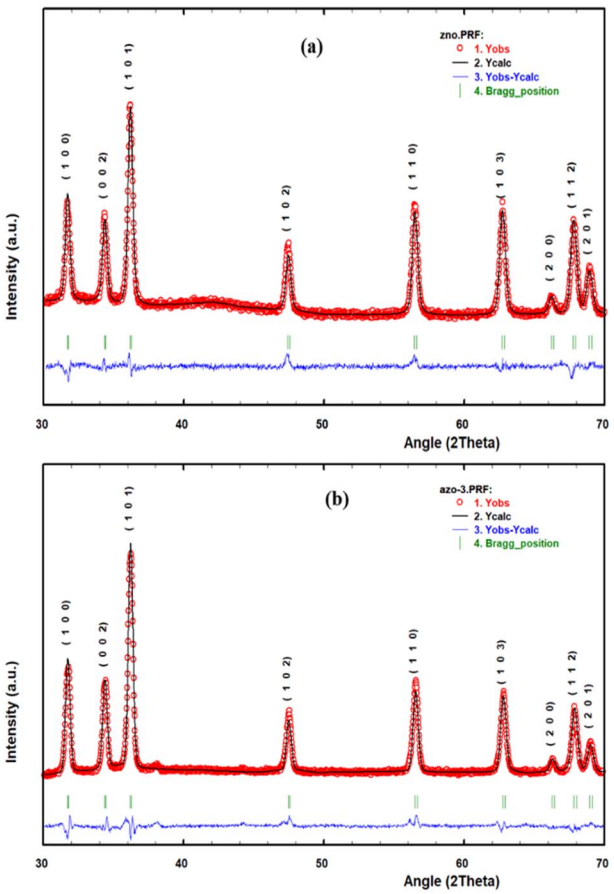

Fig. 2 Rietveld refinement of (a) Un-doped ZnO and (b) AZO-3.

Table 2 Parameters observed from Rietveld refinement

Parameters		ZnO	AZO-1	AZO-3	AZO-5	AZO-7
χ^2		1.977	2.019	3.614	5.665	7.401
Lattice parameters	*a*	3.258	3.256	3.255	3.258	3.258
	b	3.258	3.256	3.255	3.258	3.258
	c	5.219	5.217	5.214	5.218	5.219
R factors (%)	R_p	15.2	13.8	15.8	19.0	19.1
	R_{wp}	11.2	9.96	11.6	16.9	19.8
	R_e	7.93	7.01	6.10	7.08	5.88
Volume (Å^3)		47.97	47.91	47.83	47.96	47.98
Bragg *R* factor		1.87	2.26	5.26	4.46	3.04
RF factors		1.02	1.30	3.63	2.23	1.08

of more Ag ions in ZnO lattice, stress is created due to which crystallite size has reduced in AZO-3 and AZO-5.

The *d*-spacing was determined using Bragg's equation (eqn (2)).

$$2d \sin\theta = n\lambda \quad (2)$$

The dislocation density was calculated using the eqn (3) (ref. 41)

$$\delta = 1/D^2 \quad (3)$$

The microstrain was evaluated using the eqn (4) (ref. 42)

$$\varepsilon = \beta/4 \times \tan\theta \quad (4)$$

The Rietveld refinement of structural parameters was performed by full proof software. The crystal space group *P*63*mc* and Pseudo-Voigt background mode were employed with the 100 refinement cycles. As a representative of the series, the refinement plots of un-doped ZnO and AZO-3 are shown in Fig. 2, where the XRD experimental data are indicated by red circle, the fitted data by black colour line whereas the blue line indicate the difference between above two and green vertical line shows Braggs position. The output data are presented in Table 2.

Throughout the refinement process, the χ^2 shows the Goodness of fitting and the three *R*-factor show the reliability of fitting, given in the table as Profile Residual (R_p), Weighted Profile (R_{wp}) and Expected Value (R_{exp}). Rietveld analysis showed a slight decrease in *a* and *c* lattice parameter for AZO-1 and AZO-3 and after that it increased for AZO-5 and AZO-7 samples. Same trend occurred for cell volume also. This may have happened due to formation of silver nanocollection and part substitution by Ag^+ ions[28] and existence of microstructural strain from defects in Ag–ZnO.

SEM analysis

As a representative of the series, the surface morphology of both un-doped ZnO and AZO-3 NPs was analysed through SEM analysis [Fig. 3a and b]. Spherical grains were observed on the surface of both un-doped and doped samples. The average grain size was determined using ImageJ software. According to the particle distribution curve [Fig. 3c and d], the average particle

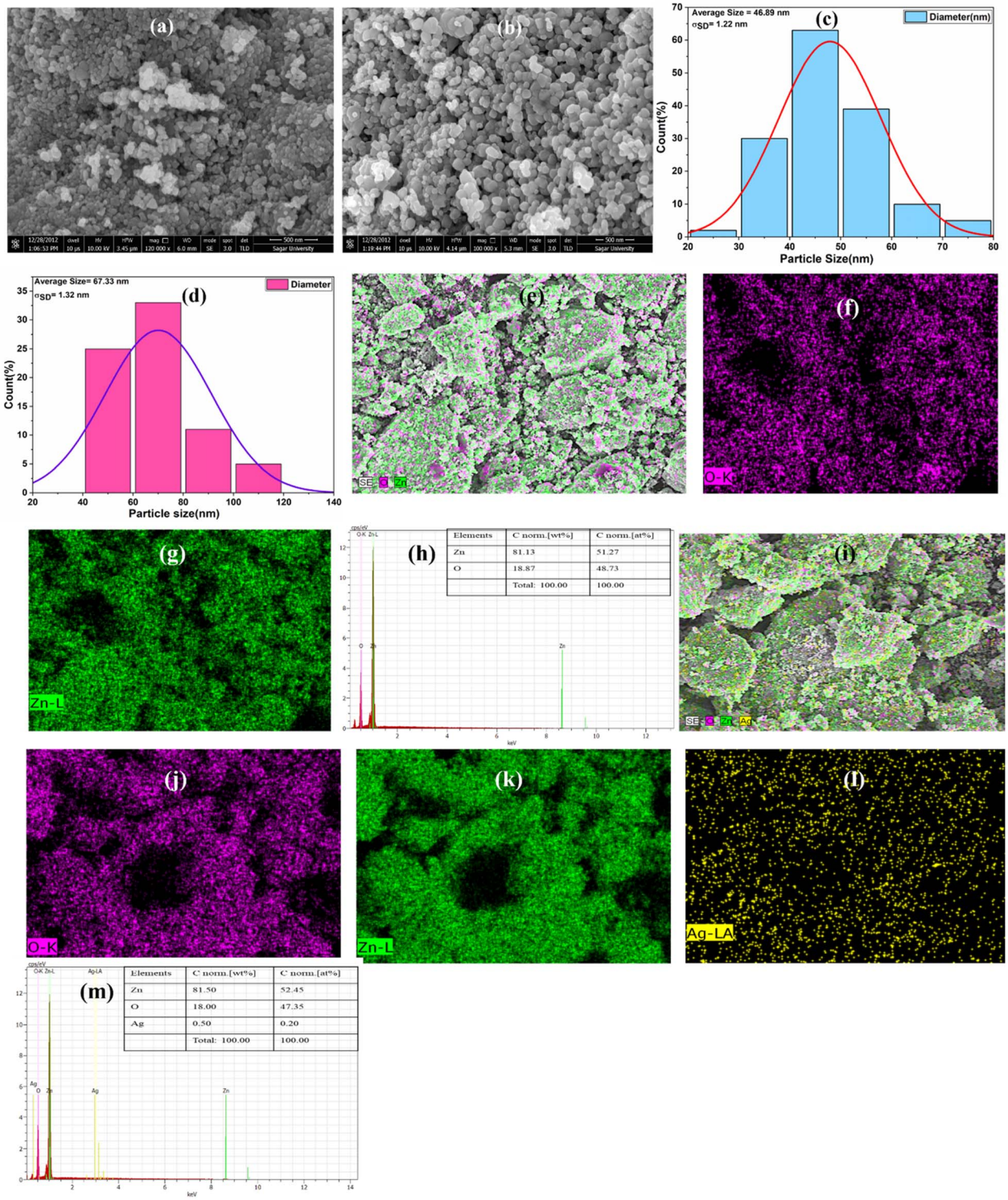

Fig. 3 SEM images of (a) un-doped ZnO and (b) AZO-3, (c and d) Particle Distributions curve, (e–m) elemental mapping of Un-doped ZnOs and AZO-3 NPs respectively.

size of un-doped ZnO and AZO-3 NPs is found to be 46.89 nm and 67.33 nm, with standard deviations σ_{SD} of 1.22 nm and 1.32 nm, respectively. The presence of elements was confirmed by the elemental mapping through EDX images [Fig. 3e–m].

TEM analysis

The microstructural image of AZO-3 nanoparticles presented in Fig. 4, was analyzed using high-resolution transmission electron microscopy (HRTEM). The TEM image of AZO-3 reveals that the synthesized nanoparticles possess a hexagonal

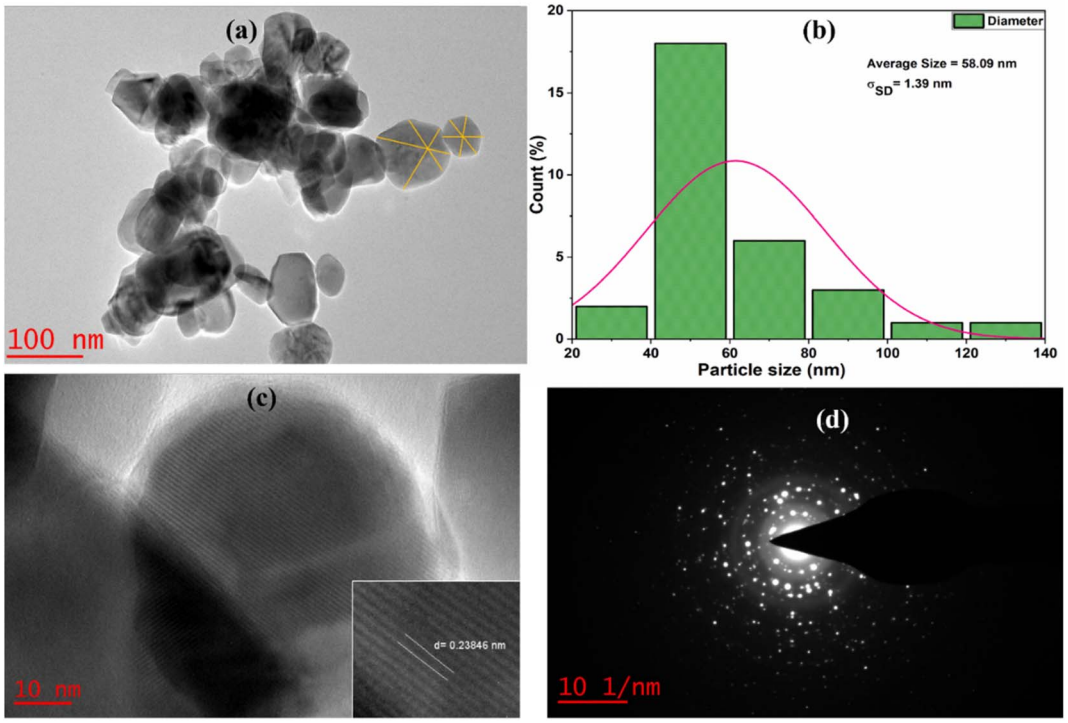

Fig. 4 (a) TEM images (b) particle distributions curve (c) HRTEM image (d) SAED image of AZO-3 NPs.

topology (a). The average particle size was calculated to be 58.09 nm, with a standard deviation of $\sigma_{SD} = 1.39$ nm (b). The HRTEM image of AZO-3 nanoparticles distinctly shows the lattice fringes (c), confirming the crystalline nature of the nanoparticles,[43] with a measured *d*-spacing of 2.3846 Å (0.23846 nm). The nanocrystalline nature of AZO-3 nanoparticles is further corroborated by the appearance of dispersed ring patterns in the selected area electron diffraction (SAED) images (d).[1]

Raman spectra analysis

The additional structural information of un-doped ZnO and Ag-doped ZnO (AZO-1 to AZO-7) was collected through Raman scattering spectra [Fig. 5]. The effect of Ag on the vibrational properties of ZnO NPs was observed. Wurtzite structure of ZnO belongs to *P*63*mc* space group. From the analysis of group theory, the modes are defined for observed peaks. The peak observed at 437 cm^{-1} attributed to E_2(high) mode confirms the wurtzite structure of ZnO.[44] On Ag doping in ZnO, the intensity of E_2 (high) phonon mode decreases indicating decrease in crystallinity due to incorporation of Ag in ZnO lattice. The E_1(LO) mode observed at 560–580 cm^{-1} is caused by defects in the ZnO lattice. These defects and disorder are introduced due to Ag incorporation in ZnO lattice.[45] The peak at 332 cm^{-1} corresponds to E_2(high)–E_2(low) mode, observed due to the second order Raman spectrum, and A_1(TO) mode and Raman

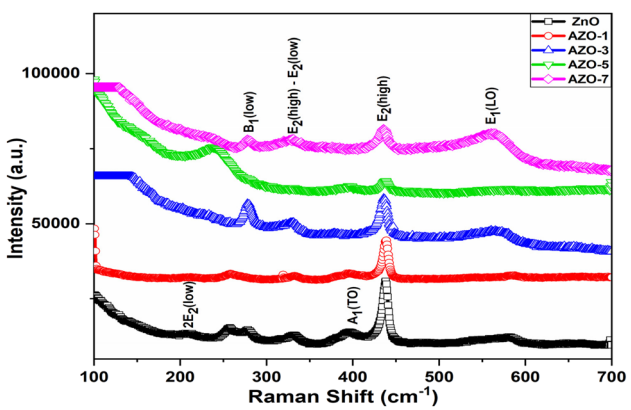

Fig. 5 Raman spectra of un-doped ZnO and Ag-doped ZnO (AZO-1 to AZO-7) NPs.

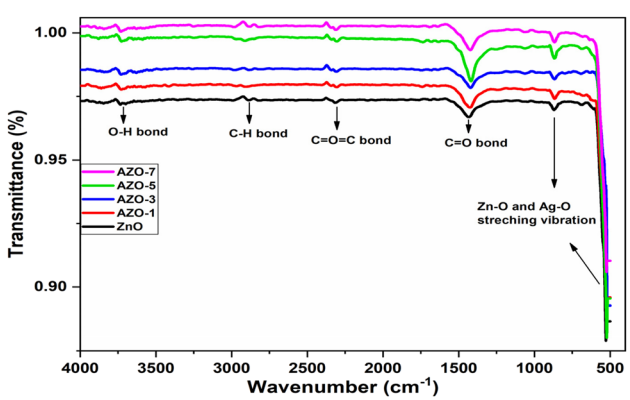

Fig. 6 FTIR spectra of un-doped ZnO and Ag-doped ZnO (AZO-1 to AZO-7) NPs.

inactive mode B_1(low) are assigned at 385 cm^{-1} and 279 cm^{-1} respectively.[46] The peak at 207 cm^{-1} assigned with $2E_2$(low) mode arises due to the vibration of oxygen atom.[47] Due to variation of defects and disorder, there is shift in peak position and change in intensity.

Fourier transform infrared (FTIR) spectra analysis

To investigate the functional group and the molecular interactions in un-doped and Ag-doped ZnO NPs FTIR spectra were analyzed in the range of 400–4000 cm^{-1} [Fig. 6]. The peaks observed at 527 cm^{-1} and 870 cm^{-1} in the un-doped ZnO NPs confirm the formation of metal oxide bond which arise due to vibrational stretching of Zn–O bond.[48] The absorption peak at 1434 cm^{-1} represents the C=O stretching mode.[49] The peak at 2886 cm^{-1} corresponds to C–H bond.[48,50] The hydroxyl group of metal oxide is present in the range of 3768–3679 cm^{-1} which arises due to stretching vibration of O–H bond[51] and the peak at 2312 cm^{-1} shows the impurity of IR spectra.[40,49] From the IR spectra the slight shift in the absorption peak with Ag doping can be associated with the substitution of Ag^+ ions in the ZnO lattice[28]

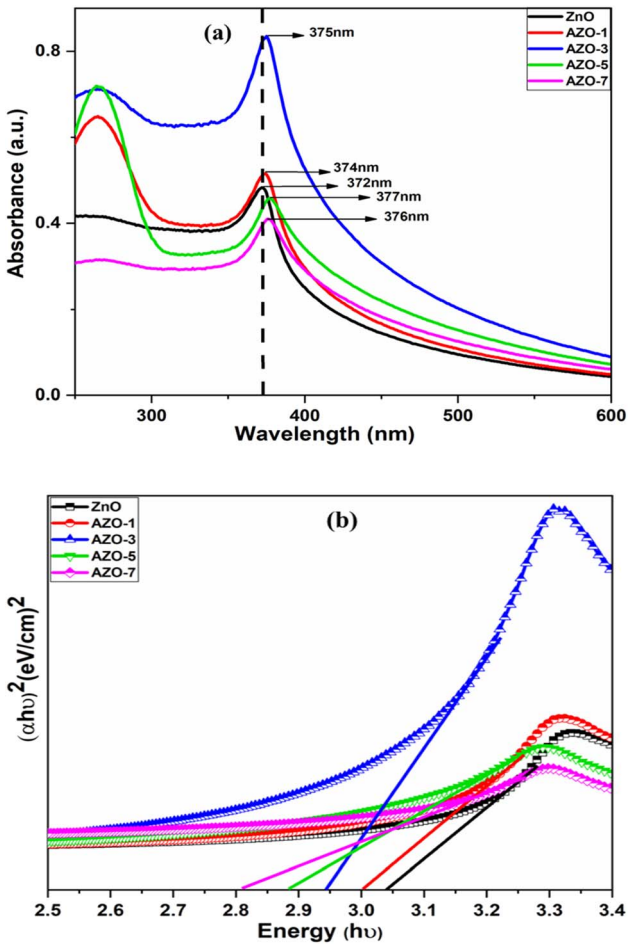

Fig. 7 (a) UV-vis absorption spectra (b) energy band gap by Tauc plot method of un-doped ZnO and Ag-doped ZnO (AZO-1 to AZO-7) NPs.

UV-visible absorption spectra analysis

Optical absorption spectra of both un-doped and Ag-doped ZnO NPs were recorded using a room temperature UV-visible spectrometer in the range of 200–600 nm [Fig. 7a]. A distinct absorption peak was observed at 372 nm for un-doped ZnO NPs. Upon Ag doping, peaks were shifted to positions 374 nm, 375 nm, 376 nm and 378 nm, for AZO-1 to AZO-7 respectively. These peaks were attributed to the excitonic absorption peak of zinc oxide nanoparticles.[52] The introduction of Ag through doping resulted in a red shift, moving the absorption edge towards higher wavelengths. The shift in absorption peak suggests a change in the energy band gap (E_g) due to the doping process. The optical energy band gap of the particles was determined using Tauc plot method.[53] This involved plotting photon energy ($h\nu$) against $(\alpha h\nu)^2$ graphs using eqn (5) and the extrapolation of the linear portion of the above graph gives the energy bandgap.

$$(\alpha h\nu)^n = A(h\nu - E_g) \quad (5)$$

where α = absorption coefficient, h = Plank's constant, ν = light frequency, A = constant, E_g is the optical bandgap, $n = 2$ for direct electronic transition and $n = 1/2$ for indirect transition.

The optical energy band gap of un-doped ZnO was measured as $E_g = 3.04$ eV. Upon the addition of Ag, the bandgap was reduced to 3.00 eV, 2.94 eV, 2.88 eV and 2.81 eV for 1% to 7% doping respectively, as illustrated in Fig. 7b. The variation in the energy band gap can be attributed to the presence of oxygen vacancies, which facilitate the electron transitions from the valence band (VB) to the conduction band (CB).[54] Due to the addition of Ag some intermediate states may have created between CB and VB in ZnO host matrix due to which band gap is reduced. Also Ag behaves like an acceptor in ZnO which lowers the band gap in Ag doped ZnO. This reduction in the energy band gap has implications for improving the optoelectronic, photocatalytic and antibacterial efficiency of the material.

Photoluminescence study

PL serves as a crucial tool for probing the optical and photochemical properties of materials, offering insights into structural imperfections such as oxygen vacancies and metal interstitials of semiconductor samples.[50] PL spectra were recorded for both un-doped ZnO and AZO nanoparticles with varying concentrations of Ag doping. The PL spectra of samples taken at room temperature are presented in Fig. 8a, in the wavelength range of 370 to 650 nm, using an excitation wavelength of 350 nm. A distinctive peak at the edge of the UV spectrum is observed around 390 nm. The UV emission is attributed to the near-band-edge (NBE) emission, indicative of free exciton recombination corresponding to the exciton–exciton collision phenomenon.[28,55] This recombination is associated with the high surface-to-volume ratio.[56] A slight shift in the peak position is noted with Ag doping, and as the doping concentration increases, the intensity decreases due to interactions among ZnO and Ag NPs at the grain boundaries. These interactions lead to a reduction in the recombination of

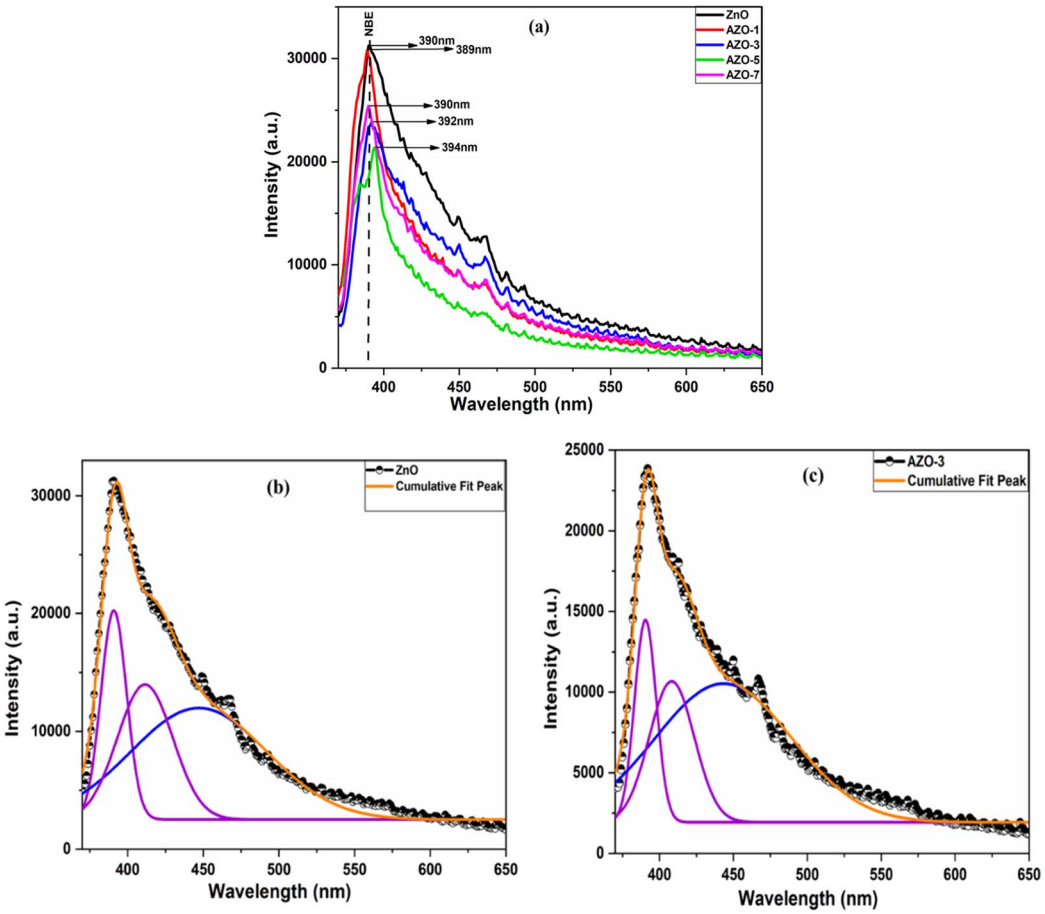

Fig. 8 (a) PL spectra of un-doped and Ag-doped ZnO NPs with excitation wavelength of 350 nm, Gaussian fitting of PL spectra of un-doped ZnO (b) and AZO-3 NPs (c).

electrons and holes.[28,57] Additionally, Ag acts as an acceptor, trapping electrons and reducing the electron–hole recombination rate, thereby decreasing the PL intensity.[58]

The spectra of ZnO and AZO-3 samples were deconvoluted by using Gaussian fitting [Fig. 8b and c]. A blue emission peak at 447 nm and 443 nm are discerned, which are due to electron

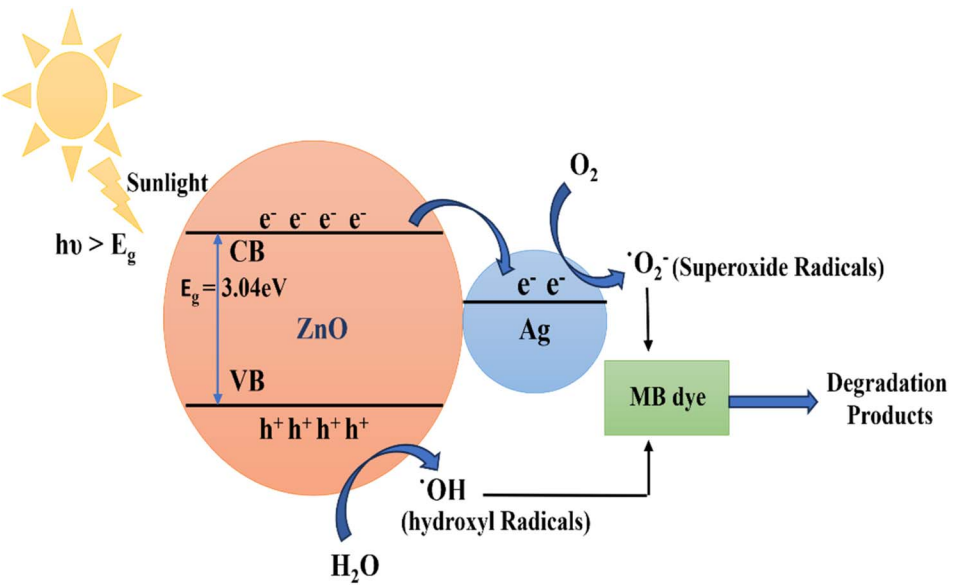

Fig. 9 Schematic diagram of Photocatalytic mechanism of Ag-doped ZnO NPs.

transition from shallow donor levels to the acceptor levels to the top level of the VB,[59] accompanied by a violet emission peak at 411 nm and 408 nm which might have arisen due to Zn vacancies (V_{Zn})[60] for un-doped ZnO and AZO-3 NPs respectively.

Photocatalytic activity

The synthesized un-doped and Ag-doped ZnO NPs are potent photocatalysts for the degradation of MB dye. The schematic diagram of photocatalytic mechanism is represented in Fig. 9. In this, the fermi energy of Ag-doped ZnO NPs is lower than that of un-doped ZnO NPs, causing electrons to move from ZnO to Ag.[61,62] Radical production is the primary mechanism behind the photodegradation of MB dye using un-doped and Ag-doped ZnO photocatalyst. The highly reactive radicals generated in the solution attack the dye molecules, resulting in less toxic by products such as water and carbon dioxide. When the

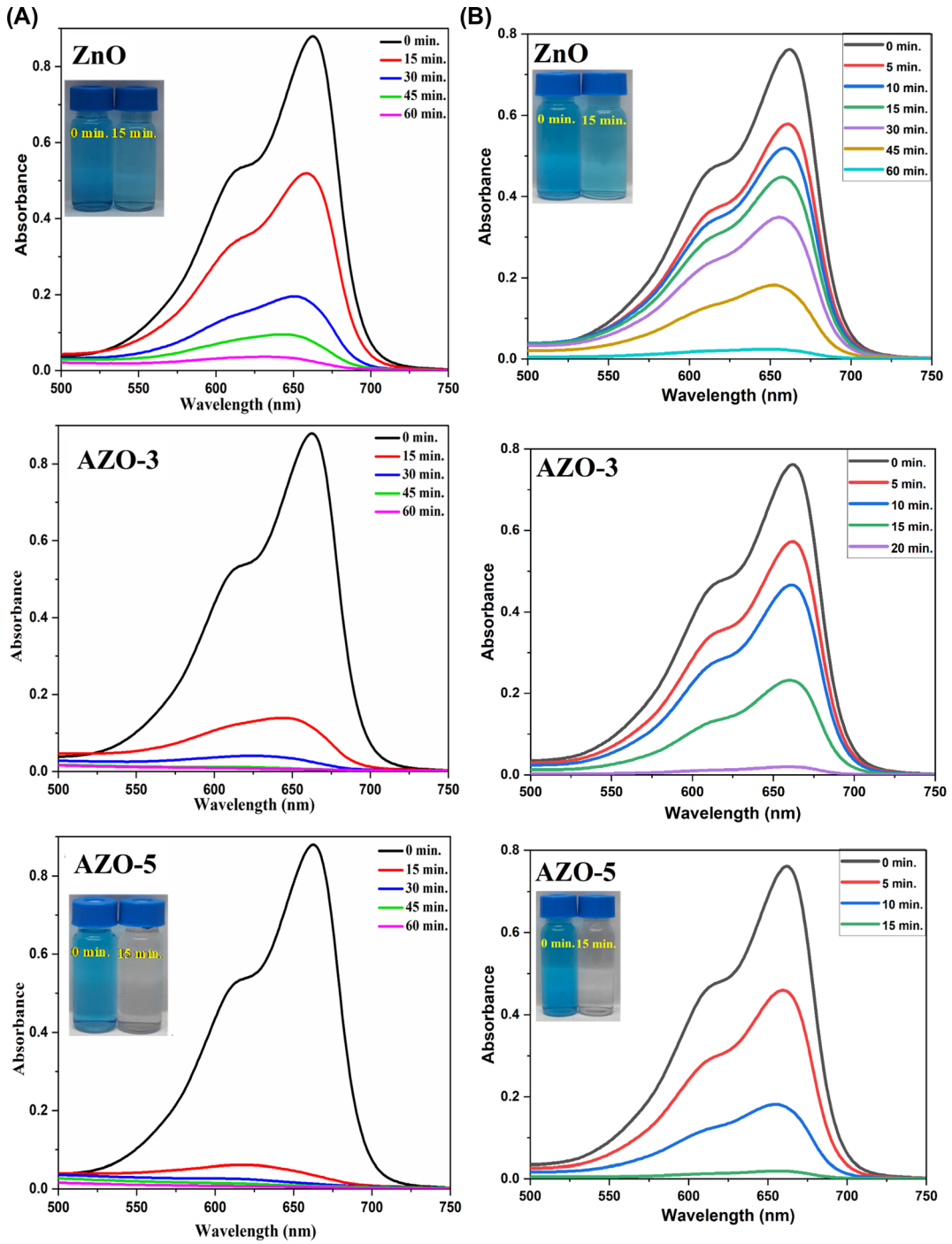

Fig. 10 (A). Photocatalytic activity of Un-doped ZnO, AZO-3 and AZO-5 NPs in degradation of MB dye under sunlight. (B) Photocatalytic activity of Un-doped ZnO, AZO-3 and AZO-5 NPs in degradation of MB dye under Xenon Short Arc lamp.

photocatalyst and dye solution are irradiated with solar light, electrons from the valence band (VB) jump to the conduction band (CB), leaving holes in the VB of the ZnO NPs. These electrons and holes serve as charge carriers for radical generation. The electrons in the conduction band react with ambient or adsorbed oxygen to form $O_2^{\bullet -}$ (superoxide anion), while the holes in the valence band react with water molecules to produce H^+ (protons) and $OH^\bullet$ (hydroxyl radicals). Similarly, the holes can react with adsorbed hydroxyl anions (OH^-) to generate additional $OH^\bullet$ radicals. These primary radicals generate further reactive oxygen species, such as $HOO^\bullet$ (peroxide radicals), $OH^\bullet$, and OH^- (hydroxyl anions). These radicals generated attack and degrade the dye molecules through reduction and oxidation processes, converting them into less harmful products like H_2O and CO_2. Hence, the electron–hole pair generation is the primary cause of dye degradation process.

In this study the photocatalytic performance of un-doped and Ag-doped ZnO NPs (AZO-3, 5) were observed through UV-visible spectra [Fig. 10A and B]. In the beginning (at 0 min) the absorbance of the solution was observed at 663 nm in the presence of the synthesized photocatalysts and both sunlight and Xenon Short Arc lamp were used as the light source, the absorbance peaks were decreased with the irradiation time. The doped ZnO photocatalysts show faster decrease in the absorbance as compared to un-doped ZnO.

The photodegradation efficiency of the prepared nanoparticles against the MB dye was calculated using eqn (6).

$$\text{Photo degradation efficiency } (\%) = (C_0 - C)/C_0\% \qquad (6)$$

where C_0 = initial concentration of MB and C = concentration of MB after degradation.

During the photo degradation of MB, under the sunlight the efficiency of ZnO was calculated to be 41.97 ± 1% after 15 min

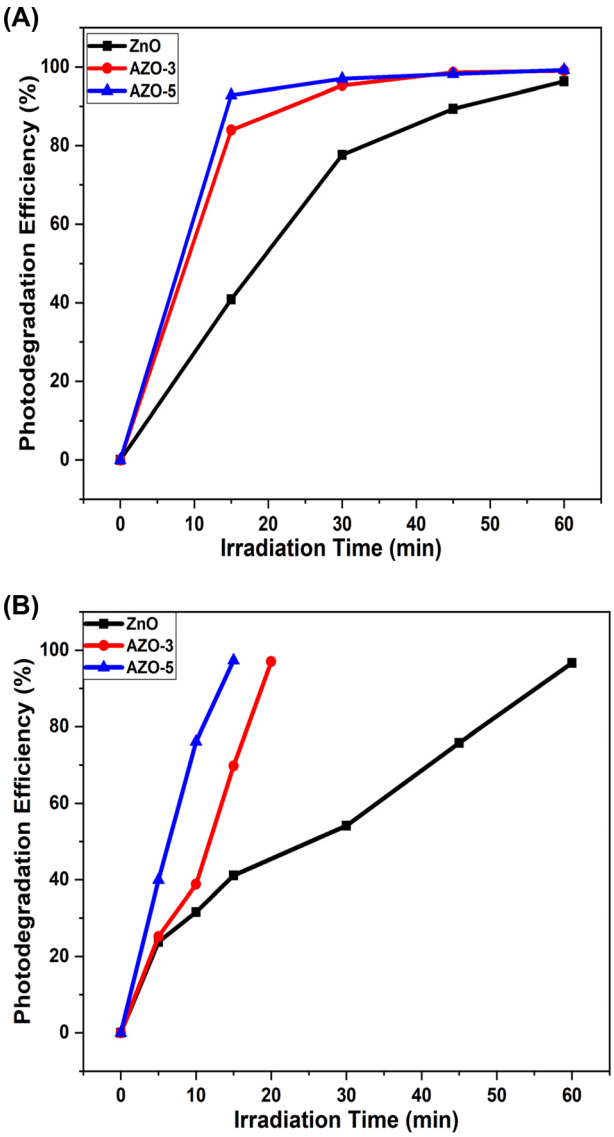

Fig. 11 (A) The photodegradation efficiency of ZnO, AZO-3 and AZO-5 with the function of irradiation time under sunlight. (B) The photodegradation efficiency of ZnO, AZO-3 and AZO-5 with the function of irradiation time under Xenon Short Arc lamp.

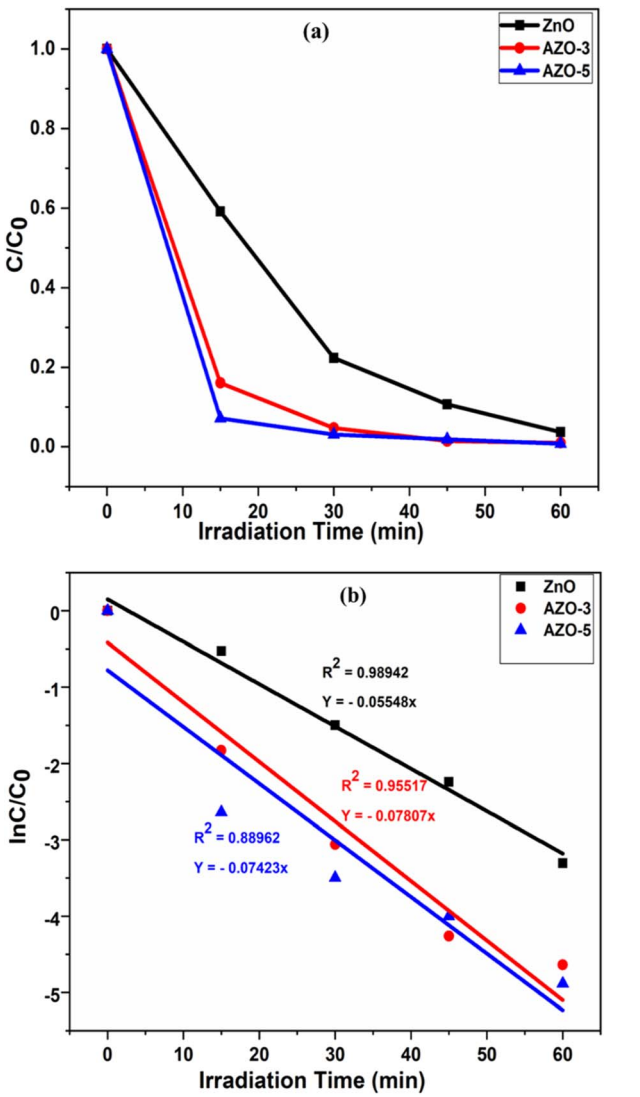

Fig. 12 (a) Dye concentration (b) photocatalyst kinetic plots of the photodegradation reaction of MB dye in the presence of catalysts ZnO, AZO-3 and AZO-5 NPs under sunlight.

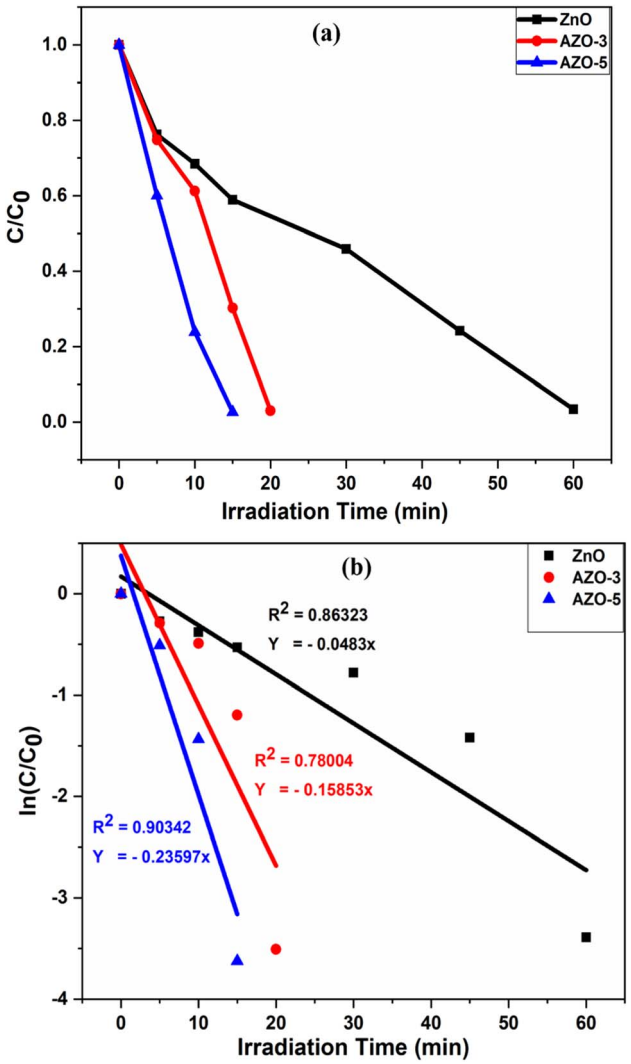

Fig. 13 (a) Dye concentration (b) photocatalyst kinetic plots of the photodegradation reaction of MB dye in the presence of catalysts ZnO, AZO-3 and AZO-5 NPs under Xenon Short Arc lamp.

of irradiation time while the efficiency of AZO-3 and AZO-5 was calculated to be 86.17 ± 1% and 96.15 ± 1% respectively in 15 min. In the short span of 45 minutes, efficiency of Ag-doped ZnO NPs was determined to be 99.12 ± 1% [Fig. 11A] which is the shortest time period ever reported till the date to the best of our knowledge. Additionally, at the same time under Xenon Short Arc lamp the efficiency of ZnO was calculated to be 96.63 ± 1% after 60 min of irradiation time while the efficiency of AZO-3 and AZO-5 was calculated to be 97.33 ± 1% in 20 min and 15 min respectively [Fig. 11B]. This demonstrates that the Ag doping in ZnO NPs increases the production of hydroxyl radicals which promotes great photocatalytic performance. The photocatalytic kinetics was employed to determine the dye concentration [Fig. 12a and 13a] and rate constants (k) for the degradation reaction of dye which follows pseudo-first order kinetics eqn (7) [Fig. 12b and 13b].

$$\ln(C/C_0) = -kt \quad (7)$$

where t = irradiation time.

The pseudo-first order plot reveals that the observed dye degradation rate constants for the catalyst AZO-3 and AZO-5 is found to be 0.07807 min^{-1} and 0.07423 min^{-1} respectively, which is higher than that of un-doped ZnO catalyst (0.0554 min^{-1}) under the sunlight [Fig. 12b]. Where the rate constant for the catalyst AZO-3 and AZO-5 is found to be 0.15853 min^{-1} and 0.23597 min^{-1} respectively, and for un-doped ZnO catalyst it is 0.0483 min^{-1} under Xenon Short Arc lamp [Fig. 13b]. So, from the degradation efficiency and kinetics it is evident that Ag-doped ZnO NPs exhibit greater photocatalytic activity in contrast to ZnO NPs which is due to lower bandgap or due to larger surface area. Incorporating Ag into ZnO reduces the recombination of photogenerated electrons and holes, thereby resulting in improved photodegradation of MB dye. The PL studies showed reduction in intensity as the doping concentration of Ag increases indicating decrease in the free charge carrier recombination which enhances

Table 3 Photocatalytic activity of Ag-doped ZnO catalyst reported from the literature

S. no.	Photocatalyst (mol/wt%)	Synthesis method	Catalyst; dye	Light source	Photodegradation efficiency (%)	Time (min)	Ref.
1	Ag–ZnO	Co-precipitation	25 mg/50 ml; 10 mg L^{-1}, MB	Halogen lamp	93%	80	63
2	Ag–ZnO	Sol–gel	0.1 g/100 ml; 2 × 10^{-5} M, MB	Visible light	82.6%	240	64
3	Ag–ZnO	Green synthesis	1.75 g L^{-1}; 20 mg L^{-1}, CR	440 W ultrasound	92.14%	60	65
4	Ag–ZnO	Co-precipitation method	20 mg/100 ml; 20 ppm/30 ml, MB	UV lamp	92.43%	150	15
5	Ag–ZnO (0.5%)	Co-precipitation	0.05 g; 10^{-5} M, MB	Visible light	98%	120	66
6	Ag–ZnO(3%)	Hydrothermal method	50 ppm/100 ml, CB dye	Visible light	65%	120	49
7	Ag–ZnO (0.14 to 0.88 wt%)	Photodeposition method	0.15 g L^{-1}; 50 mg L^{-1}, phenol	UV light	95%	180	67
8	Ag–ZnO (2.5%)	Thermal solvent	Direct blue 15	UV radiation	73.6%	120	14
9	Ag–ZnO (0–1%)	Co-precipitation method	15 mg/25 ml; 2.5 mol L^{-1}, MB	Solar light	98%	120	13
10	Ag–ZnO(3, 5%)	Wet chemical method	5 mg/50 ml; 10^{-5} M, MB	Sunlight (100 200 lux) Xenon short arc lamp	99.12% 97.33%	45 20, 15	Present work

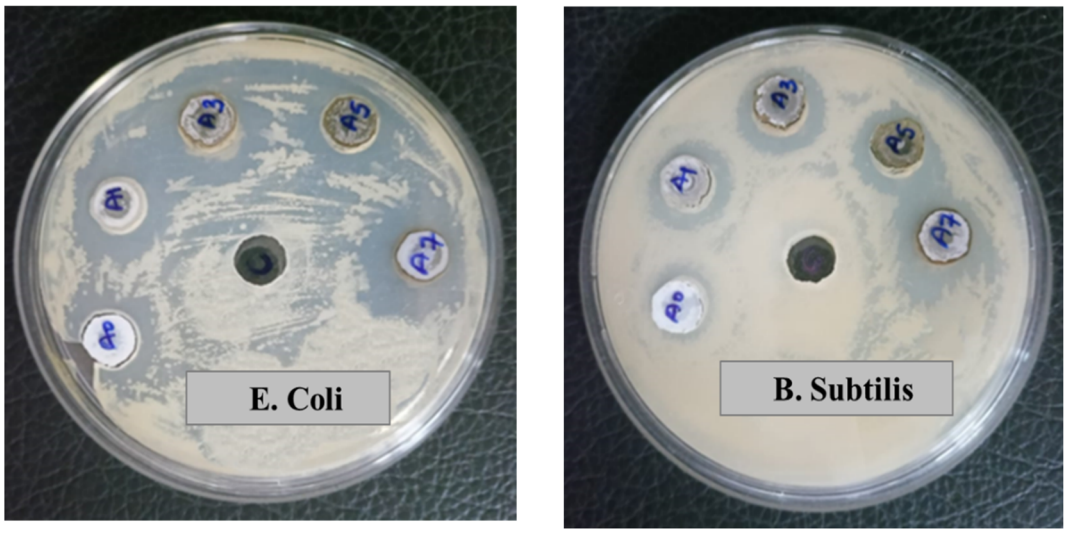

Fig. 14 Screen of un-doped and Ag-doped ZnO nanoparticles for antibacterial action against (a) *E. coli* (b) *B. subtilis* where A0 = un-doped ZnO NPs, A1 = AZO-1, A3 = AZO-3, A5 = AZO-5, A7 = AZO-7.

photocatalytic activity. Table 3 shows a comparison of literature survey on photocatalytic activity from which it is evident that our samples possess highest photodegradation efficiency in the shortest time ever reported.

Antibacterial activity

In this study, un-doped and Ag-doped ZnO NPs were investigated for their antibacterial activity against the Gram-negative bacterial strain *E. coli* and the Gram-positive strain *B. subtilis* using the Agar well diffusion method. The zone of inhibition (ZOI) around each well was measured [Fig. 14]. Table 4 illustrates that the ZOI of Ag-doped ZnO NPs has significantly increased in comparison to un-doped ZnO NPs. This enhancement is attributed to a synergistic effect that results in the production of reactive oxygen species (ROS), such as superoxide and hydroxyl radicals.[1,2,28] These reactive entities trigger oxidative stress in bacterial cells, resulting in cell damage and bacterial death. Among the tested bacterial strains, the nanoparticles exhibited the highest inhibitory activity against *E. coli*, followed by *B. subtilis*, with ZOIs of 20 mm and 18 mm, respectively, at a concentration of 25 mg ml^{-1}. The control, in contrast, showed no zone of inhibition, underscoring the inhibitory action of both un-doped and Ag-doped ZnO NPs.

Table 4 Zone of Inhibition of synthesized NPs

		Zone of inhibition (mm)	
S. no.	Synthesized NPs	*E. coli*	*B. subtilis*
1	ZnO	14	13
2	AZO-1	19	16
3	AZO-3	20	17
4	AZO-5	19	17
5	AZO-7	20	18

Conclusion

In summary, we investigated the structural, optical, photocatalytic and antibacterial properties of both un-doped and Ag-doped ZnO NPs. The samples were successfully synthesized employing a cost effective wet chemical method. The structural studies conducted by XRD, Raman spectra reveals the formation of phase pure hexagonal wurtzite structure and functional groups were analysed by FTIR spectroscopy. SEM images revealed spherical shaped NPs and HRTEM images showed the nanocrytalline nature of synthesized nanoparticles having diameter of 58.09 nm and calculated *d*-spacing of 2.3846 Å justifying the SEM and XRD results respectively. The optical properties were investigated through UV-vis and PL spectra. From UV-vis spectra, a reduction in energy band gap is observed with increase in Ag doping. The alteration in the energy band gap value relies on diverse factors, such as crystallite size and the placement of the dopant within the host lattice. With increase in Ag doping concentration, the free charge carrier recombination is decreased as observed in the PL spectra. The variations in the structural and optical properties of Ag-doped ZnO NPs, compared to un-doped ZnO NPs, contributed to the excellent photocatalytic and antibacterial activity. The photocatalytic study shows highest degradation efficiency of 99.12 ± 1% in the span of 45 min under sunlight and 97.33 ± 1% in 15 min under Xenon Short Arc lamp which are the shortest time ever reported. Therefore, Ag-doped ZnO NPs find extensive applications in waste water treatments and pharmaceutical manufacturing.

Data availability

The corresponding author (Dr Anupama Chanda) confirms that whenever required we will provide the original data used in this manuscript.

Author contributions

The first author (Vaishali Amrute) has contribution in methodology, investigation and original draft writing. Second author (Monika) has contributed in data curation. Third author (K. K. Supin) has contribution in data curation and investigation and editing. Fourth author (M. Vasundhara) has contribution in investigation, review and editing. Fifth author (Anupama chanda) has contribution in conceptualization, supervision, review and editing.

Conflicts of interest

The authors declare that there is no conflict of interest.

Acknowledgements

The first author (Vaishali Amrute) Acknowledges UGC-DAE CSR, Indore for RAMAN analysis, Department of Microbiology for antibacterial study and the Centre for Advanced Research (CAR) of Dr. Harisingh Gour Vishwavidyalaya, Sagar (M.P.) (A Central University) for XRD, SEM and TEM analysis. M. Vasundhara would like to acknowledge the support offered by Department of K & IM of Indian Institute of Chemical Technology (IICT/Pubs./2024/350).

References

1 I. H. Ifijen, M. Maliki and B. Anegbe, Synthesis, Photocatalytic Degradation and Antibacterial Properties of Selenium or Silver Doped Zinc Oxide Nanoparticles: A Detailed Review, *OpenNano*, 2022, **8**, 100082, DOI: **10.1016/j.onano.2022.100082**.

2 N. Sharma, J. Kumar, S. Thakur, S. Sharma and V. Shrivastava, Antibacterial Study of Silver Doped Zinc Oxide Nanoparticles against Staphylococcus Aureus and *Bacillus Subtilis*, *Drug Invent. Today*, 2013, **5**(1), 50–54, DOI: **10.1016/j.dit.2013.03.007**.

3 J. X. Wang, X. W. Sun, A. Wei, Y. Lei, X. P. Cai, C. M. Li and Z. L. Dong, Zinc Oxide Nanocomb Biosensor for Glucose Detection, *Appl. Phys. Lett.*, 2006, **88**(23), 233106, DOI: **10.1063/1.2210078**.

4 L. Demarconnay, E. Raymundo-Piñero and F. Béguin, Adjustment of Electrodes Potential Window in an Asymmetric Carbon/MnO2 Supercapacitor, *J. Power Sources*, 2011, **196**(1), 580–586, DOI: **10.1016/j.jpowsour.2010.06.013**.

5 S. Das and V. Jayaraman, SnO2: A Comprehensive Review on Structures and Gas Sensors, *Prog. Mater. Sci.*, 2014, **66**, 112–255, DOI: **10.1016/j.pmatsci.2014.06.003**.

6 A. Chanda, S. R. Joshi, V. R. Akshay, S. Varma, J. Singh, M. Vasundhara and P. Shukla, Structural and Optical Properties of Multilayered Un-Doped and Cobalt Doped TiO2 Thin Films, *Appl. Surf. Sci.*, 2021, **536**, 147830, DOI: **10.1016/j.apsusc.2020.147830**.

7 A. Chanda, K. Rout, M. Vasundhara, S. R. Joshi and J. Singh, Structural and Magnetic Study of Undoped and Cobalt Doped TiO_2 Nanoparticles, *RSC Adv.*, 2018, **8**(20), 10939–10947, DOI: **10.1039/C8RA00626A**.

8 C. Ruttanapun, W. Prachamon and A. Wichainchai, Optoelectronic Properties of $Cu_{1-x}Pt_xFeO_2$ ($0 \leq x \leq 0.05$) Delafossite for p-Type Transparent Conducting Oxide, *Curr. Appl. Phys.*, 2012, **12**(1), 166–170, DOI: **10.1016/j.cap.2011.05.028**.

9 A. Chanda, S. Gupta, M. Vasundhara, S. R. Joshi, G. R. Mutta and J. Singh, Study of Structural, Optical and Magnetic Properties of Cobalt Doped ZnO Nanorods, *RSC Adv.*, 2017, **7**(80), 50527–50536, DOI: **10.1039/C7RA08458G**.

10 X. Wang, R. Zheng, Z. Liu, H. Ho, J. Xu and S. P. Ringer, Structural, Optical and Magnetic Properties of Co-Doped ZnO Nanorods with Hidden Secondary Phases, *Nanotechnology*, 2008, **19**(45), 455702, DOI: **10.1088/0957-4484/19/45/455702**.

11 N. A. F. Al-Rawashdeh, O. Allabadi and M. T. Aljarrah, Photocatalytic Activity of Graphene Oxide/Zinc Oxide Nanocomposites with Embedded Metal Nanoparticles for the Degradation of Organic Dyes, *ACS Omega*, 2020, **5**(43), 28046–28055, DOI: **10.1021/acsomega.0c03608**.

12 S. Gautam, H. Agrawal, M. Thakur, A. Akbari, H. Sharda, R. Kaur and M. Amini, Metal Oxides and Metal Organic Frameworks for the Photocatalytic Degradation: A Review, *J. Environ. Chem. Eng.*, 2020, **8**(3), 103726, DOI: **10.1016/j.jece.2020.103726**.

13 M. A. Kareem, I. T. Bello, H. A. Shittu, P. Sivaprakash, O. Adedokun and S. Arumugam, Synthesis, Characterization, and Photocatalytic Application of Silver Doped Zinc Oxide Nanoparticles, *Cleaner Mater.*, 2022, **3**, 100041, DOI: **10.1016/j.clema.2022.100041**.

14 R. Ebrahimi, K. Hossienzadeh, A. Maleki, R. Ghanbari, R. Rezaee, M. Safari, B. Shahmoradi, H. Daraei, A. Jafari, K. Yetilmezsoy and S. H. Puttaiah, Effects of Doping Zinc Oxide Nanoparticles with Transition Metals (Ag, Cu, Mn) on Photocatalytic Degradation of Direct Blue 15 Dye under UV and Visible Light Irradiation, *J. Environ. Health Sci. Eng.*, 2019, **17**(1), 479–492, DOI: **10.1007/s40201-019-00366-x**.

15 S. Mangala Nagasundari, K. Muthu, K. Kaviyarasu, D. A. A. Farraj and R. M. Alkufeidy, Current Trends of Silver Doped Zinc Oxide Nanowires Photocatalytic Degradation for Energy and Environmental Application, *Surf. Interfaces*, 2021, **23**(1), 100931, DOI: **10.1016/j.surfin.2021.100931**.

16 A. P. Manuel, S. Riddell, H. Rajashekhar, D. Vrushabendrakumar, K. M. Alam, P. Kumar, S. Gusarov, A. E. Kobryn, M. Supur, R. L. McCreery and K. Shankar, Hot Carrier Photocatalysis Using Bimetallic Au@Pt Hemispherical Core–Shell Nanoislands, *J. Mater. Sci.: Mater. Electron.*, 2022, **33**(22), 18134–18155, DOI: **10.1007/s10854-022-08671-2**.

17 D. Vrushabendrakumar, H. Rajashekhar, S. Riddell, A. P. Kalra, K. M. Alam and K. Shankar, Synthesis, Characterization, and Visible Light Photocatalytic Activity of Solution-Processed Free-Standing 2D Bi_2O_2Se Nanosheets, *Nanotechnology*, 2021, **32**(48), 485602, DOI: **10.1088/1361-6528/ac1753**.

18 Ş. Ş. Türkyılmaz, N. Güy and M. Özacar, Photocatalytic Efficiencies of Ni, Mn, Fe and Ag Doped ZnO Nanostructures Synthesized by Hydrothermal Method: The Synergistic/Antagonistic Effect between ZnO and Metals, *J. Photochem. Photobiol., A*, 2017, **341**, 39–50, DOI: 10.1016/j.jphotochem.2017.03.027.

19 M. A. Qamar, M. Javed and S. Shahid, Designing and Investigation of Enhanced Photocatalytic and Antibacterial Properties of 3d (Fe, Co, Ni, Mn and Cr) Metal-Doped Zinc Oxide Nanoparticles, *Opt. Mater.*, 2022, **126**, 112211, DOI: 10.1016/j.optmat.2022.112211.

20 J. bo Zhong, J. zhang Li, X. yang He, J. Zeng, Y. Lu, W. Hu and K. Lin, Improved Photocatalytic Performance of Pd-Doped ZnO, *Curr. Appl. Phys.*, 2012, **12**(3), 998–1001, DOI: 10.1016/j.cap.2012.01.003.

21 C. A. Jaramillo-Páez, J. A. Navío, M. C. Hidalgo and M. Macías, ZnO and Pt-ZnO Photocatalysts: Characterization and Photocatalytic Activity Assessing by Means of Three Substrates, *Catal. Today*, 2018, **313**, 12–19, DOI: 10.1016/j.cattod.2017.12.009.

22 T. K. Pathak, R. E. Kroon and H. C. Swart, Photocatalytic and Biological Applications of Ag and Au Doped ZnO Nanomaterial Synthesized by Combustion, *Vacuum*, 2018, **157**, 508–513, DOI: 10.1016/j.vacuum.2018.09.020.

23 K. Qi, B. Cheng, J. Yu and W. Ho, Review on the Improvement of the Photocatalytic and Antibacterial Activities of ZnO, *J. Alloys Compd.*, 2017, **727**, 792–820, DOI: 10.1016/j.jallcom.2017.08.142.

24 R. Wang, J. H. Xin, Y. Yang, H. Liu, L. Xu and J. Hu, The Characteristics and Photocatalytic Activities of Silver Doped ZnO Nanocrystallites, *Appl. Surf. Sci.*, 2004, **227**(1–4), 312–317, DOI: 10.1016/j.apsusc.2003.12.012.

25 R. Rajendran and A. Mani, Photocatalytic, Antibacterial and Anticancer Activity of Silver-Doped Zinc Oxide Nanoparticles, *J. Saudi Chem. Soc.*, 2020, **24**(12), 1010–1024, DOI: 10.1016/j.jscs.2020.10.008.

26 A. H. Habeeb, Alshamsi and S. Hussein Batool, Hydrothermal Preparation of Silver Doping Zinc Oxide Nanoparticles: Studys, Characterization and Photocatalytic Activity, *Orient. J. Chem.*, 2018, **34**(4), 1898–1907, DOI: 10.13005/ojc/3404025.

27 R. Chauhan, A. Kumar and R. P. Chaudhary, Photocatalytic Studies of Silver Doped ZnO Nanoparticles Synthesized by Chemical Precipitation Method, *J. Sol-Gel Sci. Technol.*, 2012, **63**(3), 546–553, DOI: 10.1007/s10971-012-2818-3.

28 S. M. Hosseini, I. A. Sarsari, P. Kameli and H. Salamati, Effect of Ag Doping on Structural, Optical, and Photocatalytic Properties of ZnO Nanoparticles, *J. Alloys Compd.*, 2015, **640**, 408–415, DOI: 10.1016/j.jallcom.2015.03.136.

29 G. Nagaraju, S. Udayabhanu, S. A. Prashanth, M. Shastri, K. V. Yathish, C. Anupama and D. Rangappa, Electrochemical Heavy Metal Detection, Photocatalytic, Photoluminescence, Biodiesel Production and Antibacterial Activities of Ag–ZnO Nanomaterial, *Mater. Res. Bull.*, 2017, **94**, 54–63, DOI: 10.1016/j.materresbull.2017.05.043.

30 R. Rajendran and A. Mani, Photocatalytic, Antibacterial and Anticancer Activity of Silver-Doped Zinc Oxide Nanoparticles, *J. Saudi Chem. Soc.*, 2020, **24**(12), 1010–1024, DOI: 10.1016/j.jscs.2020.10.008.

31 P. Panchal, R. Sharma, A. Sudharshan Reddy, K. Nehra, A. Sharma and S. P. Nehra, Eco-Friendly Synthesis of Ag-Doped ZnO/MgO as a Potential Photocatalyst for Antimicrobial and Dye Degradation Applications, *Coord. Chem. Rev.*, 2023, **493**, 215283, DOI: 10.1016/j.ccr.2023.215283.

32 M. K. Seery, R. George, P. Floris and S. C. Pillai, Silver Doped Titanium Dioxide Nanomaterials for Enhanced Visible Light Photocatalysis, *J. Photochem. Photobiol., A*, 2007, **189**(2–3), 258–263, DOI: 10.1016/j.jphotochem.2007.02.010.

33 T. Chitradevi, A. Jestin Lenus, J. Victor and N. Structure, Morphology and Luminescence Properties of Sol-Gel Method Synthesized Pure and Ag-Doped ZnO Nanoparticles, *Mater. Res. Express*, 2020, **7**(1), 015011, DOI: 10.1088/2053-1591/ab5c53.

34 N. Khadgi, Y. Li, A. R. Upreti, C. Zhang, W. Zhang, Y. Wang and D. Wang, Enhanced Photocatalytic Degradation of 17 α-Ethinylestradiol Exhibited by Multifunctional $ZnFe_2O_4$–Ag/rGO Nanocomposite Under Visible Light, *Photochem. Photobiol.*, 2016, **92**(2), 238–246, DOI: 10.1111/php.12565.

35 C. Abinaya, M. Marikkannan, M. Manikandan, J. Mayandi, P. Suresh, V. Shanmugaiah, C. Ekstrum and J. M. Pearce, Structural and Optical Characterization and Efficacy of Hydrothermal Synthesized Cu and Ag Doped Zinc Oxide Nanoplate Bactericides, *Mater. Chem. Phys.*, 2016, **184**, 172–182, DOI: 10.1016/j.matchemphys.2016.09.039.

36 L. Muñoz-Fernandez, A. Sierra-Fernandez, G. Flores-Carrasco, O. Milošević and M. E. Rabanal, Solvothermal Synthesis of Ag/ZnO Micro/Nanostructures with Different Precursors for Advanced Photocatalytic Applications, *Adv. Powder Technol.*, 2017, **28**(1), 83–92, DOI: 10.1016/j.apt.2016.09.033.

37 F. Khurshid, M. Jeyavelan, M. S. L. Hudson and S. Nagarajan, Ag-Doped ZnO Nanorods Embedded Reduced Graphene Oxide Nanocomposite for Photo-Electrochemical Applications, *R. Soc. Open Sci.*, 2019, **6**(2), 181764, DOI: 10.1098/rsos.181764.

38 L. A. Gusmão, D. A. Peixoto, J. Z. Marinho, F. C. Romeiro, R. F. Gonçalves, E. Longo, C. A. de Oliveira and R. C. Lima, Alkali Influence on ZnO and Ag-Doped ZnO Nanostructures Formation Using the Microwave-Assisted Hydrothermal Method for Fungicidal Inhibition, *J. Phys. Chem. Solids*, 2021, **158**, 110234, DOI: 10.1016/j.jpcs.2021.110234.

39 C. Karunakaran, V. Rajeswari and P. O. Gomathisankar, Electrical, Photocatalytic, and Bactericidal Properties of Microwave Synthesized Nanocrystalline Ag–ZnO and ZnO, *Solid State Sci.*, 2011, **13**(5), 923–928, DOI: 10.1016/j.solidstatesciences.2011.02.016.

40 M. B. Islam, M. J. Haque, N. M. Shehab and M. S. Rahman, Synthesis and Characterization (Optical and Antibacterial) of Silver Doped Zinc Oxide Nanoparticles, *Open Ceram.*, 2023, **14**, 100370, DOI: 10.1016/j.oceram.2023.100370.

41 R. Radičić, D. Maletić, D. Blažeka, J. Car and N. Krstulović, Synthesis of Silver, Gold, and Platinum Doped Zinc Oxide Nanoparticles by Pulsed Laser Ablation in Water, *Nanomaterials*, 2022, **12**(19), 3484, DOI: 10.3390/nano12193484.

42 P. Shunmuga Sundaram, T. Sangeetha, S. Rajakarthihan, R. Vijayalaksmi, A. Elangovan and G. Arivazhagan, XRD Structural Studies on Cobalt Doped Zinc Oxide Nanoparticles Synthesized by Coprecipitation Method: Williamson-Hall and Size-Strain Plot Approaches, *Phys. B*, 2020, **595**, 412342, DOI: 10.1016/j.physb.2020.412342.

43 Ö. A. Yıldırım, H. E. Unalan and C. Durucan, Highly Efficient Room Temperature Synthesis of Silver-Doped Zinc Oxide (ZnO:Ag) Nanoparticles: Structural, Optical, and Photocatalytic Properties, *J. Am. Ceram. Soc.*, 2013, **96**(3), 766–773, DOI: 10.1111/jace.12218.

44 O. Lupan, V. Cretu, V. Postica, M. Ahmadi, B. R. Cuenya, L. Chow, I. Tiginyanu, B. Viana, T. Pauporté and R. Adelung, Silver-Doped Zinc Oxide Single Nanowire Multifunctional Nanosensor with a Significant Enhancement in Response, *Sens. Actuators, B*, 2016, **223**, 893–903, DOI: 10.1016/j.snb.2015.10.002.

45 L. Shen, N. Bao, K. Yanagisawa, K. Domen, A. Gupta and C. A. Grimes, Direct Synthesis of ZnO Nanoparticles by a Solution-Free Mechanochemical Reaction, *Nanotechnology*, 2006, **17**(20), 5117–5123, DOI: 10.1088/0957-4484/17/20/013.

46 I. Musa, N. Qamhieh and S. T. Mahmoud, Synthesis and Length Dependent Photoluminescence Property of Zinc Oxide Nanorods, *Results Phys.*, 2017, **7**, 3552–3556, DOI: 10.1016/j.rinp.2017.09.035.

47 B. H. Bairamov, A. Heinrich, G. Irmer, V. V. Toporov and E. Ziegler, Raman Study of the Phonon Halfwidths and the Phonon—Plasmon Coupling in ZnO, *Phys. Status Solidi B*, 1983, **119**(1), 227–234, DOI: 10.1002/pssb.2221190126.

48 A. J. Lafta, A. Alsultani, A. S. Farhood, A. M. Odeh, A. S. Ferhod and A. J. Lafta, *Modification of the Photocatalytic Activity of Zinc Oxide by Doping Silver*, 2014. https://www.researchgate.net/publication/268576951.

49 H. A. Habeeb Alshamsi and B. S. Hussein, Hydrothermal Preparation of Silver Doping Zinc Oxide Nanoparticles: Studys, Characterization and Photocatalytic Activity, *Orient. J. Chem.*, 2018, **34**(4), 1898–1907, DOI: 10.13005/ojc/3404025.

50 R. Georgekutty, M. K. Seery and S. C. Pillai, A Highly Efficient Ag-ZnO Photocatalyst: Synthesis, Properties, and Mechanism, *J. Phys. Chem. C*, 2008, **112**(35), 13563–13570, DOI: 10.1021/jp802729a.

51 S. Bashir, M. S. Awan, M. A. Farrukh, R. Naidu, S. A. Khan, N. Rafique, S. Ali, I. Hayat, I. Hussain and M. Z. Khan, In-Vivo (Albino Mice) and in-Vitro Assimilation and Toxicity of Zinc Oxide Nanoparticles in Food Materials, *Int. J. Nanomed.*, 2022, **17**, 4073–4085, DOI: 10.2147/IJN.S372343.

52 R. Saravanan, N. Karthikeyan, V. K. Gupta, E. Thirumal, P. Thangadurai, V. Narayanan and A. Stephen, ZnO/Ag Nanocomposite: An Efficient Catalyst for Degradation Studies of Textile Effluents under Visible Light, *Mater. Sci. Eng., C*, 2013, **33**(4), 2235–2244, DOI: 10.1016/j.msec.2013.01.046.

53 V. Kumar, J. Prakash, J. P. Singh, K. H. Chae, C. Swart, O. M. Ntwaeaborwa, H. C. Swart and V. Dutta, Role of Silver Doping on the Defects Related Photoluminescence and Antibacterial Behaviour of Zinc Oxide Nanoparticles, *Colloids Surf., B*, 2017, **159**, 191–199, DOI: 10.1016/j.colsurfb.2017.07.071.

54 K. Jyoti and A. Singh, Green Synthesis of Nanostructured Silver Particles and Their Catalytic Application in Dye Degradation, *J. Genet. Eng. Biotechnol.*, 2016, **14**(2), 311–317, DOI: 10.1016/j.jgeb.2016.09.005.

55 S. Thambidurai, P. Gowthaman, M. Venkatachalam and S. Suresh, Enhanced Bactericidal Performance of Nickel Oxide-Zinc Oxide Nanocomposites Synthesized by Facile Chemical Co-Precipitation Method, *J. Alloys Compd.*, 2020, **830**, 154642, DOI: 10.1016/j.jallcom.2020.154642.

56 W. Q. Peng, S. C. Qu, G. W. Cong and Z. G. Wang, Structure and Visible Luminescence of ZnO Nanoparticles, *Mater. Sci. Semicond. Process.*, 2006, **9**(1–3), 156–159, DOI: 10.1016/j.mssp.2006.01.038.

57 Y. Jin, Q. Cui, K. Wang, J. Hao, Q. Wang and J. Zhang, Investigation of Photoluminescence in Undoped and Ag-Doped ZnO Flowerlike Nanocrystals, *J. Appl. Phys.*, 2011, **109**(5), 053521, DOI: 10.1063/1.3549826.

58 N. R. Khalid, Z. Hong, E. Ahmed, Y. Zhang, H. Chan and M. Ahmad, Synergistic Effects of Fe and Graphene on Photocatalytic Activity Enhancement of TiO2 under Visible Light, *Appl. Surf. Sci.*, 2012, **258**(15), 5827–5834, DOI: 10.1016/j.apsusc.2012.02.110.

59 A. A. Othman, M. A. Osman, E. M. M. Ibrahim and M. A. Ali, Sonochemically Synthesized ZnO Nanosheets and Nanorods: Annealing Temperature Effects on the Structure, and Optical Properties, *Ceram. Int.*, 2017, **43**(1), 527–533, DOI: 10.1016/j.ceramint.2016.09.189.

60 S.-H. Jeong, B.-S. Kim and B.-T. Lee, Photoluminescence Dependence of ZnO Films Grown on Si(100) by Radio-Frequency Magnetron Sputtering on the Growth Ambient, *Appl. Phys. Lett.*, 2003, **82**(16), 2625–2627, DOI: 10.1063/1.1568543.

61 M. Zare, K. Namratha, S. Alghamdi, Y. H. E. Mohammad, A. Hezam, M. Zare, Q. A. Drmosh, K. Byrappa, B. N. Chandrashekar, S. Ramakrishna and X. Zhang, Novel Green Biomimetic Approach for Synthesis of ZnO-Ag Nanocomposite; Antimicrobial Activity against Food-Borne Pathogen, Biocompatibility and Solar Photocatalysis, *Sci. Rep.*, 2019, **9**(1), 8303, DOI: 10.1038/s41598-019-44309-w.

62 A. Ziashahabi, M. Prato, Z. Dang, R. Poursalehi and N. Naseri, The Effect of Silver Oxidation on the Photocatalytic Activity of Ag/ZnO Hybrid Plasmonic/Metal-Oxide Nanostructures under Visible Light and in the Dark, *Sci. Rep.*, 2019, **9**(1), 11839, DOI: 10.1038/s41598-019-48075-7.

63 R. S. Sabry, M. I. Rahmah and W. J. Aziz, A Systematic Study to Evaluate Effects of Stearic Acid on Superhydrophobicity and Photocatalytic Properties of Ag-Doped ZnO

Nanostructures, *J. Mater. Sci.: Mater. Electron.*, 2020, **31**(16), 13382–13391, DOI: **10.1007/s10854-020-03893-8**.

64 M. F. Abdel Messih, M. A. Ahmed, A. Soltan and S. S. Anis, Synthesis and Characterization of Novel Ag/ZnO Nanoparticles for Photocatalytic Degradation of Methylene Blue under UV and Solar Irradiation, *J. Phys. Chem. Solids*, 2019, **135**, 109086, DOI: **10.1016/j.jpcs.2019.109086**.

65 Y. Y. Chan and Y. L. Pang and S. Lim and W. C. Chong, Sonocatalytic Degradation of Congo Red by Using Green Synthesized Silver Doped Zinc Oxide Nanoparticles, in *Materials Today: Proceedings*, Elsevier Ltd, 2020, Vol. 46, pp. 1948–1953. DOI: **10.1016/j.matpr.2021.02.242**.

66 R. Mohammadzadeh Kakhki, R. Tayebee and F. Ahsani, New and Highly Efficient Ag Doped ZnO Visible Nano Photocatalyst for Removing of Methylene Blue, *J. Mater. Sci.: Mater. Electron.*, 2017, **28**(8), 5941–5952, DOI: **10.1007/s10854-016-6268-5**.

67 V. Vaiano, M. Matarangolo, J. J. Murcia, H. Rojas, J. A. Navío and M. C. Hidalgo, Enhanced Photocatalytic Removal of Phenol from Aqueous Solutions Using ZnO Modified with Ag, *Appl. Catal., B*, 2018, **225**, 197–206, DOI: **10.1016/j.apcatb.2017.11.075**.